SUBMILLIMETER CONTINUUM OBSERVATIONS OF 2060 CHIRON

DAVID JEWITT[1]
Institute for Astronomy, University of Hawaii, 2680 Woodlawn Drive, Honolulu, Hawaii 96822

JANE LUU[1]
Center for Astrophysics, Harvard University, 60 Garden Street, Cambridge, Massachusetts 02138

Received 18 November 1991; revised 18 March 1992

ABSTRACT

We present new submillimeter photometry of 2060 Chiron taken at the James Clerk Maxwell Telescope on Mauna Kea. The measurements are used to constrain the diameter of Chiron. Submillimeter wavelengths fall in the Rayleigh–Jeans portion of the blackbody spectrum of the nucleus, and are relatively insensitive to surface temperature uncertainties. These wavelengths are also insensitive to small dust particles in the coma. We find a 3σ upper limit to the 800 μm flux density equal to 11 mJy. The photometry is interpreted using an analytic model of the submillimeter emission, and a numerical model which takes conduction into account. With either model, we find a 3σ upper limit to the diameter $d \leqslant 300$ km. This is consistent with, but smaller than, the 372 km upper limit obtained by Sykes & Walker [Science, 251, 777 (1991)] based on photometry at shorter wavelengths. Submillimeter photometry provides a strong and relatively model-independent observational constraint on the size of the nucleus.

1. INTRODUCTION

The object 2060 Chiron exhibits cometary characteristics while at large heliocentric distances, $R \geqslant 10\ AU$ (Hartmann *et al.* 1990; Luu & Jewitt 1990; Meech & Belton 1990). Scientific interest in 2060 Chiron is focused both on the nature of this low-temperature activity, and on the origin of Chiron itself. For instance, the orbit is unstable to planetary perturbations on timescales $\sim 10^5$ yr. It is possible that Chiron is the largest of a set of comets evolving into the planetary region from the hypothesized Kuiper Belt (Duncan *et al.* 1988). On the other hand, Hahn & Bailey (1990) showed that Chiron may be evolving *outwards* from a previously smaller short-period orbit. In short, both the physical nature and the past history of Chiron are intriguing mysteries.

The nucleus of 2060 Chiron is widely believed to be larger than the nuclei of other short-period comets. This belief is based primarily on the bright absolute magnitude determined from observations at large distances. The faintest (i.e., least coma-contaminated) reported magnitude is $H_v = 6.8 \pm 0.1$ (Bus *et al.* 1991). In the H, G magnitude system as described by Bowell *et al.* (1989), the H_v magnitude is related to the visual geometric albedo, p, and diameter, d [km], by

$$\log d = 3.130 - 0.2\ H_v - 0.5 \log p\ . \qquad (1)$$

For example, with a comet-like albedo $p = 0.02$, the diameter implied by Eq. (1) is $d \sim 420$ km. However, with an albedo similar to that of the Jovian satellite Callisto, namely, $p \sim 0.20$, the derived diameter shrinks to $d \sim 130$ km, and at the albedo of the icy Saturnian satellite Enceladus, $p \sim 1.0$, we find $d \sim 60$ km. Evidently, the bright H_v magnitude of Chiron only constrains the nucleus diameter in the range $60 \leqslant d \leqslant 420$ km. If some fraction of the light is contributed by coma, then these diameters must be regarded as upper limits. For comparison, the diameter of the next largest known cometary nucleus (P/Schwassman–Wachmann 1) is estimated at $d \sim 40$ km (Cruikshank & Brown 1983; Jewitt 1990).

Unfortunately, while it seems likely that Chiron does indeed possess a relatively large nucleus, there exist no reliable measurements of its size. The nucleus size is important in several respects. Depending on the size, the surface gravity might be sufficient to influence the motions of ejected gas and dust (Banaszkiewicz *et al.* 1990). As the largest known nucleus, Chiron influences our perception of the comet nucleus size distribution.

Lebofsky *et al.* (1984) published a 2σ upper limit to the flux density at 22 μm wavelength, $F_{22} = 17 \pm 9$ mJy (1 mJy $= 10^{-29}$ W m^{-2} Hz^{-1}). They interpreted F_{22} using the standard asteroid thermal model (described in Lebofsky *et al.* 1986) and reported a Chiron nucleus diameter $d \sim 180$ km and albedo $p \sim 0.1$. However, the application of the standard asteroid thermal model to Chiron was criticized by Spencer *et al.* (1989) and by Sykes & Walker (1991).

In the standard asteroid thermal model, incident solar energy is assumed to be absorbed and emitted from a single hemisphere of the nucleus, while conduction into the interior is neglected. This assumption is reasonable for the asteroids, where small heliocentric distances and high surface temperatures lead to rapid blackbody cooling on the antisolar hemisphere. However, at the distance of 2060 Chiron, cooling by blackbody radiation is very slow, and the temperature on the night side of a rapid rotator may be comparable with that on the day side (Spencer *et al.* 1989).

[1]Visiting Astronomer at the James Clerk Maxwell Telescope, operated by the Royal Observatory Edinburgh on behalf of the Science and Engineering Research Council of the United Kingdom, The Netherlands Organization for Scientific Research, and the National Research Council of Canada.

 0004-6256/92/070398-07$00.90

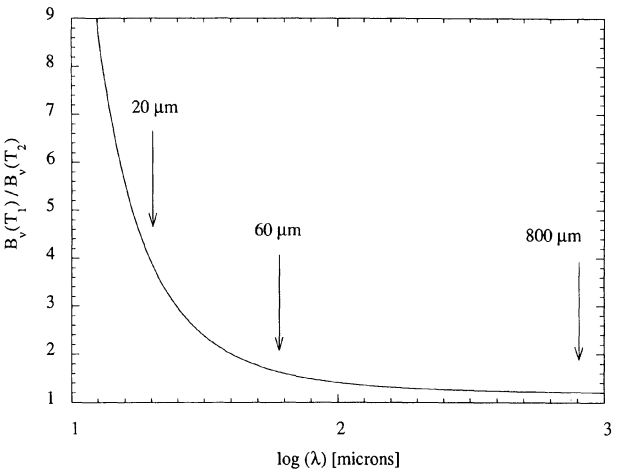

FIG. 1. Ratio of Planck functions at temperatures $T_1=100$ K and $T_2=84$ K. Vertical lines at 20, 60, and 800 μm mark the approximate wavelengths available to ground-based near-infrared (Lebofsky *et al.* 1984), space-based far-infrared (Sykes & Walker 1991), and submillimeter (this work) observations. A fractional temperature uncertainty $(T_2-T_1/T_1\sim 16\%$ produces 20 μm flux densities in the ratio 4:1, and renders the derived nucleus cross section uncertain by a factor of 4.

In the latter case, the mean day-side temperature will be less than in the standard asteroid model. As an illustration, in Fig. 1 we show the ratio of two blackbody spectra computed for Chiron temperatures predicted by the standard model ($T_1=100$ K) and by an isothermal model ($T_2=84$ *K*). The $\sim 16\%$ temperature difference between these models produces 20 μm flux densities different in the ratio 4:1. In this case, the imperfect knowledge of the surface temperature distribution leads to an uncertainty in the derived nucleus cross section of a factor of order 4. Thus, measurements at wavelengths on the Wien side of the blackbody maximum are subject to large uncertainties of interpretation. For instance, the Lebofsky *et al.* measurements were reassessed by Sykes & Walker (1991), who found a 3σ limit to the diameter $d\leqslant 204$ km using the standard asteroid thermal model. However, they also reported that the diameter could be as large as $d\leqslant 600$ km, if nucleus rotation efficiently carries day-time heat onto the night side, leading to a latitude-isothermal nucleus. Sykes & Walker obtained a stronger constraint from *IRAS* photometry at 60 μm, namely, $d\leqslant 372$ km, under the isothermal approximation, and assuming an infrared emissivity $\epsilon_{IR}=0.9$. Spencer *et al.* (1989) speculated that the nucleus could be as large as 400 km in diameter. The essential point is that the interpretation of Wien region photometry is critically sensitive to the nucleus temperature distribution, and that the latter is inherently uncertain because the nucleus spin vector of Chiron is unknown.

In this paper, we present new submillimeter photometry of Chiron, and show that it provides a relatively model-independent upper limit to the size. Submillimeter wavelengths fall in the Rayleigh–Jeans region of the blackbody emission from the nucleus. In this region, the emitted flux is a weak function of nucleus temperature, so that uncertainties in the nucleus temperature exert less impact on the interpretation of the photometry.

2. OBSERVATIONS

Submillimeter observations of 2060 Chiron were taken in 1990 November and 1991 March, using the James Clerk Maxwell Telescope (JCMT) located on Mauna Kea. This is a 15 m diameter telescope capable of diffraction limited imaging down to 350 μm wavelength. The common user bolometer UKT14 (Duncan *et al.* 1990) was used for all observations. This single-element photometer was used in conjunction with a filter having a central wavelength $\lambda=800$ μm and fractional full width at half-maximum $\Delta\lambda/\lambda=0.25$. At this wavelength, the diffraction limited angular resolution is $\theta\sim 14''$. We employed a 65 mm diameter circular diaphragm at the Nasmyth focus, corresponding to 18″ in the plane of the sky. Background subtraction was achieved by chopping to a sky position 40″ from the object in azimuth, at a frequency 7.8 Hz. The choice of the chop distance is a compromise between small distances, which place the chop position on the wings of the diffraction spot, and large distances, which chop to distant, and therefore, less relevant, areas of sky. The telescope was also periodically beam switched, to remove possible asymmetries between the two projected beams.

The Chiron ephemeris was obtained using a program provided by David Tholen. The accuracy of this program was independently checked by optical observations from the University of Hawaii 2.2 m telescope (Luu & Annis 1991). Their observations on UT 1991 March 7 showed that the instantaneous predicted and measured positions of Chiron were consistent to better than 2″. In 1990 November, Chiron was moving with respect to the fixed stars at 2.1″/ hr, while in 1991 March the motion had decreased to 1.8″/hr. This motion was followed using telescope control software to linearly interpolate between hourly starting and ending ephemeris positions. Absolute pointing of the JCMT was determined by maximizing the submillimeter signal on nearby objects of well-known position. These included Mars, 0754+100, 0735+178, IRC+10°216, and 3C279 (Sandell 1992). From comparison of the pointing measurements, we found that the uncertainty of the JCMT position was not greater than ±2″—a small fraction of the 18″ diameter beam.

Astronomical observations at 800 μm are highly susceptible to the water content of the terrestrial atmosphere. The present observations of Chiron were taken on two nights characterized by low 800 μm opacity, low sky noise, and minimal anomalous refraction. Flux calibration was obtained using nearby submillimeter flux standards, including Mars, the primary standard at these wavelengths. The 800 μm Mars flux within the JCMT beam was taken to be 3493 Jy on UT 1990 November 4, and 617 Jy on UT 1991 March 22. In addition to Mars, we used IRC+10°216, 0754+100, and 0735+178 as intermediate standards. Because the submillimeter sky is spatially and temporally variable, observations of flux standards were repeated approximately every 45 min throughout the course of the

TABLE 1. 800 μm photometry of 2060 Chiron.

U T Date (1)	R(AU) (2)	Δ(AU) (3)	α(°) (4)	F_ν (mJy) (5)	F_ν (mJy) (6)
1990 November 04	10.73	10.45	−5.2	6.2±4.8	<14.4
1991 March 22	10.48	10.09	5.1	1.2±6.0	<18.0
Combined	10.48	10.09	5.1	4.2±3.7	<11.1

Notes to TABLE 1

(1) Date of observation.
(2) Heliocentric distance in Astronomical Units.
(3) Geocentric distance in Astronomical Units.
(4) Phase angle in degrees.
(5) Measured flux density in milli-Janskys.
(6) Equivalent 3σ upper limits to the flux density in milli-Janskys.

observations. Photometric uncertainties estimated from the observations of standards were ±10%.

The observational results are summarized in Table 1. There it may be seen that Chiron was not detected above 3 standard deviations at 800 μm, on either night of observation. We combined the two measurements in quadrature to obtain the final limit on the 800 μm flux density, also listed in the table.

3. INTERPRETATION OF THE SUBMILLIMETER DATA

We present two descriptions of our interpretation of the submillimeter photometry. The analytic model in Sec. *3.1* involves some simplifying approximations but is physically revealing. The exact model in Sec. *3.2* is based on a numerical solution to the conduction equation on the surface of a rotating sphere of arbitrary obliquity.

3.1 Simple Model of the Submillimeter Emission

Consider a spherical nucleus on which the surface distribution of temperature is $T(\theta,\phi)$, where θ,ϕ are polar angles such that θ is the angular distance from the subsolar point and ϕ is an azimuthal angle. The thermal flux density received by an observer at distance Δ[m] and at zero phase angle is

$$F_\nu = \int B_\nu[T(\theta,\phi)]\epsilon_\nu \, d\Omega \,, \tag{2}$$

where $d\Omega$ [sr] is the solid angle subtended by the surface element at position θ,ϕ, $B_\nu[T(\theta,\phi)]$ [W m^{-2} Hz^{-1} sr^{-1}] is the Planck function evaluated at the temperature of the surface at position θ, ϕ, and ϵ_ν is the emissivity at frequency ν [Hz]. The integration is carried out over the entire visible hemisphere of the body. The solution of Eq. (2) depends entirely on knowing $T(\theta,\phi)$ and ϵ_ν. For a sphere of radius, r[m], viewed at zero-phase angle, we have

$$d\Omega = \frac{2\pi r^2 \sin\theta\cos\theta \, d\theta}{\Delta^2} \,. \tag{3}$$

The surface temperature distribution, $T(\theta,\phi)$, is influenced by the thermal and spin characteristics of the body. Among the important characteristics are the Bond albedo and infrared emissivity of the surface, the thermal diffusivity of the surface material (which controls the rate of conduction of heat into the deep interior), and the magnitude and direction of the spin vector. In the case of 2060 Chiron, of these characteristics, only the spin period is known with confidence. The spin period is important since rapid rotation can carry day-time heat to the night side, leading to more nearly isothermal surface temperatures than on a nonspinning or slowly spinning body (Spencer *et al.* 1989). This effect is especially important on Chiron, where the surface temperatures and the radiation-cooling rates are small compared to their values on main-belt asteroids.

In the Rayleigh–Jeans limit ($hc \ll \lambda kT$) the Planck function approximates

$$B_\nu(T) \sim \frac{2kT}{\lambda^2} \,, \tag{4}$$

and Eq. (2) may be written as

$$F_\nu = \frac{2k\overline{T}}{\lambda^2}\epsilon_\nu\frac{\pi r^2}{\Delta^2} \,, \tag{5}$$

where $\overline{T}$ is the average temperature on the visible hemisphere weighted by solid angle and given by

$$\overline{T} = \frac{\int_\Omega T(\theta,\phi)d\Omega}{\int_\Omega d\Omega} \,. \tag{6}$$

The value of $\overline{T}$ is a function of the nucleus spin vector. For a nonrotating, nonconducting body in thermal equilibrium, the temperature at a point where the solar zenith angle is ψ may be computed from

$$\frac{F_{\rm Sun}(1-A)\cos\psi}{R^2} = \epsilon_{\rm IR}\sigma T^4(\theta,\phi) \,. \tag{7}$$

In Eq. (7), $F_{\rm Sun}$=1360 W m^2 is the solar constant, A is the bond albedo, $\epsilon_{\rm IR}$ the infrared emissivity, $\sigma = 5.67\times10^{-8}$ W m^{-2} K^{-4} is Stefan's constant, and R [AU] is the heliocentric distance. It is convenient to express the surface temperature in terms of the subsolar temperature on the nonrotating nucleus, namely,

$$T(0,0) = \left(\frac{F_{\rm Sun}(1-A)}{\epsilon_{\rm IR}\sigma R^2}\right)^{1/4} \,. \tag{8}$$

Substitution of Eq. (7) into Eq. (6) then yields

$$\overline{T} = \frac{T(0,0)}{\chi^{1/4}} \,, \tag{9}$$

with χ=1.6. For the case of an isothermal nucleus, the mean temperature is given by Eq. (9) with χ=4. Thus, these extreme examples of possible thermal regimes result in mean temperatures in the ratio $(4/1.6)^{1/4}\sim1.26$.

By combining Eqs. (5, 8, and 9), we obtain an expression for the diameter of a body producing a given submillimeter flux density

$$d = \left(\frac{2F_\nu}{\pi k\epsilon_{\rm sm}}\right)^{1/2}\lambda\Delta\left(\frac{\sigma R^2}{F_{\rm Sun}}\right)^{1/8}\left(\frac{\epsilon_{\rm IR}\chi}{1-A}\right)^{1/8} \,. \tag{10}$$

Equation (10) is remarkably insensitive to the unknowns $\epsilon_{\rm IR}$, χ, and A (where lies the primary advantage of the submillimeter wavelengths for size estimation). For exam-

TABLE 2. Submillimeter emissivities of icy bodies.

Object (1)	λ (2)	F_{pred} (3)	F_{obs} (4)	ϵ_{sm} (5)	Reference
Ganymede	1.3	10.34	8.8 ± 0.8	0.85 ± 0.08	Ulich *et al.* (1984)
Callisto	1.3	9.4	9.8 ± 0.5	1.04 ± 0.05	Ulich *et al.* (1984)
Pluto	1.2	20.8×10^{-3}	$(17\pm2)\times10^{-3}$ [a]	0.82 ± 0.10	Altenhoff *et al.* (1988)

[a]Includes pointing correction factor 1.15.

Notes to TABLE 2

(1) Object name.
(2) Wavelength of observation in millimeters.
(3) Flux density (Jy) predicted from known radius, distance, and temperature of the object.
(4) Observed flux density (Jy).
(5) Effective emissivity, computed from column 4 divided by column 3.

ple, an uncertainty of a factor of 2 in these quantities produces a relative error in the derived diameter of $\Delta d/d = 2^{1/8}-1=9\%$. The derived diameter is more sensitive to the submillimeter emissivity, ϵ_{sm}. The submillimeter emissivities of various outer solar system bodies are summarized in Table 2. There it may be seen that the mean submillimeter emissivity is of order $\epsilon_{sm}=0.9\pm0.1$. In the absence of any theory for the submillimeter emissivity, we employ these empirical values as our best estimate for ϵ_{sm}. The error on the diameter resulting from this uncertainty in ϵ_{sm} is about $\pm6\%$.

In Table 3, we present values of the diameter, d, derived from Eq. (10). Several diameters are computed for various assumed values of A, ϵ_{IR}, χ and ϵ_{sm}, as listed in the table. The table shows that the submillimeter data are consistent with Chiron diameters as large as 330 km, when interpreted using the simple model.

Notice that the analytic model involves several approximations. For instance, the Planck function is approximated by the Rayleigh–Jeans law [Eq. (4)]. This assumption is valid at the relatively high temperature of the subsolar point on Chiron, but becomes suspect at the lower temperatures found near the Chiron terminator. Therefore, we are motivated to consider a more detailed model of the thermal emission to test the significance of the approximations employed in the analytic model.

TABLE 3. Diameter constraints from the analytic model.

A (1)	ϵ_{IR} (2)	ϵ_{sm} (3)	χ (4)	$\left(\frac{\epsilon_{IR}\chi}{1-A}\right)^{1/8}$ (5)	d(km) (6)
0.0	1.0	1.0	1.6	1.06	$\leqslant$270
0.0	1.0	1.0	4.0	1.19	$\leqslant$302
0.1	1.0	1.0	4.0	1.20	$\leqslant$304
0.1	0.8	0.8	4.0	1.17	$\leqslant$332
0.5	1.0	1.0	1.6	1.16	$\leqslant$294
0.5	1.0	1.0	4.0	1.30	$\leqslant$330
0.5	0.5	0.8	1.6	1.06	$\leqslant$301

Notes to TABLE 3

(1) Bond Albedo.
(2) Infrared emissivity.
(3) Submillimeter emissivity.
(4) Spin parameter.
(5) Self-evident.
(6) Derived 3σ upper limit to the nucleus diameter [km].

3.2 *Conduction Model of the Submillimeter Emission*

As a check on the preceding approximate calculation, we computed a more detailed model of the distribution of surface temperature on 2060 Chiron. The full calculation of the surface temperature is based on the energy balance equation including conduction but neglecting sublimation,

$$\rho c_p \frac{\partial T}{\partial t}=\frac{\partial}{\partial z}\left(k\frac{\partial T}{\partial z}\right), \tag{11}$$

where k [W m^{-1} K^{-1}] is the thermal conductivity, ρ [kg m^{-3}] is the mass density, and c_p [J kg^{-1}K^{-1}] is the specific heat capacity. The neglect of sublimation energy in Eq. (11) is permitted by the tiny mass loss rates inferred in 2060 Chiron to date [e.g., Luu & Jewitt (1990) found $dm/dt\sim1$ kg s^{-1}].

The surface boundary condition for the solution of Eq. (11) is expressed by the condition that the solar energy absorbed by the top layer be equal to the sum of the energies radiated into space and conducted into the interior, namely,

$$\frac{F_{Sun}(1-A)\cos\psi}{R^2}=\epsilon\sigma T^4+k\left.\frac{\partial T}{\partial z}\right|_0, \tag{12}$$

where $(\partial T/\partial z|_0)$ is the instantaneous surface temperature gradient. Note that for a given point on the surface, ψ is a function of time due to diurnal rotation of the body. Except in special cases, the solution of Eqs. (11) and (12) for the surface temperature must be obtained numerically.

We solved Eq. (11) using the Crank–Nicholson finite-difference method (Press *et al.* 1986) on a Sun 4/65 SPARCstation. Calculations were done using 90 equal-width latitude bands spanning between the poles. Experiments showed that use of a larger number of latitude bands did not change the model results. The vertical transfer of energy into the nucleus was calculated using a set of slabs, each of thickness 0.1–0.25 times the diurnal thermal skin depth. The number of discrete longitude steps was chosen to ensure convergence of the model. Depending on helio-

centric distance and spin period, the number of longitude steps varied from 600 to 12 000. The model Chiron was given a spin period $P=5.917\,80$ hr (Luu & Jewitt 1990), and a range of surface thermal properties. The stability of each model with respect to the choice of slab thicknesses and time increments was carefully checked.

The thermal inertia $I=(k\rho c_p)^{1/2}$ is unknown for Chiron. As a guide, the Moon has $I\sim 50$ MKS units (Winter & Saari 1969), where 1 MKS unit $=\mathrm{J\,K^{-1}\,m^{-2}s^{-1/2}}$, Mars has $65\leqslant I\leqslant 460$ MKS (Kieffer *et al.* 1977), and the Martian satellites Phobos and Deimos have $25\leqslant I\leqslant 85$ MKS (Lunine *et al.* 1982). The lower values are characteristic of dust and may be representative of the expected low density surface of Chiron. Furthermore, at the low temperatures found on Chiron ($T<100$ K) we expect to find smaller I, since c_p decreases with decreasing T (see, e.g., Fig. 1 of Winter & Saari 1969). We computed solutions to the heat diffusion equation for a range of thermal properties and orientations of the nucleus. To explore the sensitivity of the results to the assumed thermal inertia, we computed models using $I=10$, 50, and 250 MKS. The orientation of the spin axis of the nucleus of 2060 Chiron is unknown. In this paper, we describe results from models in which the subsolar latitude is $\theta_{ss}=0°$ (i.e., Chiron is viewed from an equatorial perspective), $\theta_{ss}=45°$, and $\theta_{ss}=90°$ (i.e., the polar axis points at the Sun). For simplicity, we assume that the phase angle is zero (cf. Table 1), and the models were computed using the heliocentric and geocentric distances of Chiron on UT 1991 March 22 (see Table 1).

Isotherms for representative models having different subsolar latitudes are plotted in Fig. 2. At 0° subsolar latitude [Fig 2(a)], the temperature is diurnally variable, with a maximum following the local noon and a minimum near sunrise. The amplitude of the diurnal temperature variation at a given latitude depends on the thermal inertia, but is typically very small. At $\theta_{ss}=90°$ [Fig. 2(c)] the temperature is constant along lines of fixed latitude, with a maximum at the pole $T(0,0)\sim 120$ K. This temperature is in good agreement with Eq. (9). The models from Fig. 2 are shown pictorially in Fig. 3 [Plate 77], with color coding such that temperatures run from white (120 K) to blue (80 K). Figure 4 shows results for three models with $\theta_{ss}=0°$, and with $I=10$, 50, and 250 MKS units. Curve (b) in the figure shows that the diurnal temperature variation is $\Delta T\sim 12$ K, for $I=50$ MKS. This is small compared to the maximum $T(0,0)\sim 98$ K for this thermal inertia. Conversely, in the low inertia model [$I=10$ MKS, curve (c)], the day–night temperature contrast enlarges to $\Delta T\sim 40$ K, compared to a peak $T(0,0)\sim 112$ K. Thus, the thermal models show that, unless the thermal inertia is very small, the rapid rotation and large heliocentric distance of 2060 Chiron, together tend to produce a small day–night temperature contrast. Notice from Fig. 4 that, as a result of thermal lag, the temperature maximum shifts to larger longitudes as the thermal inertia increases.

The temperatures obtained from the conduction model were used to compute the flux density emitted at zero phase angle, using Eq. (2), with adopted infrared and submillimeter emissivities ϵ_{IR} and $\epsilon_{sm}=0.9$. The flux density

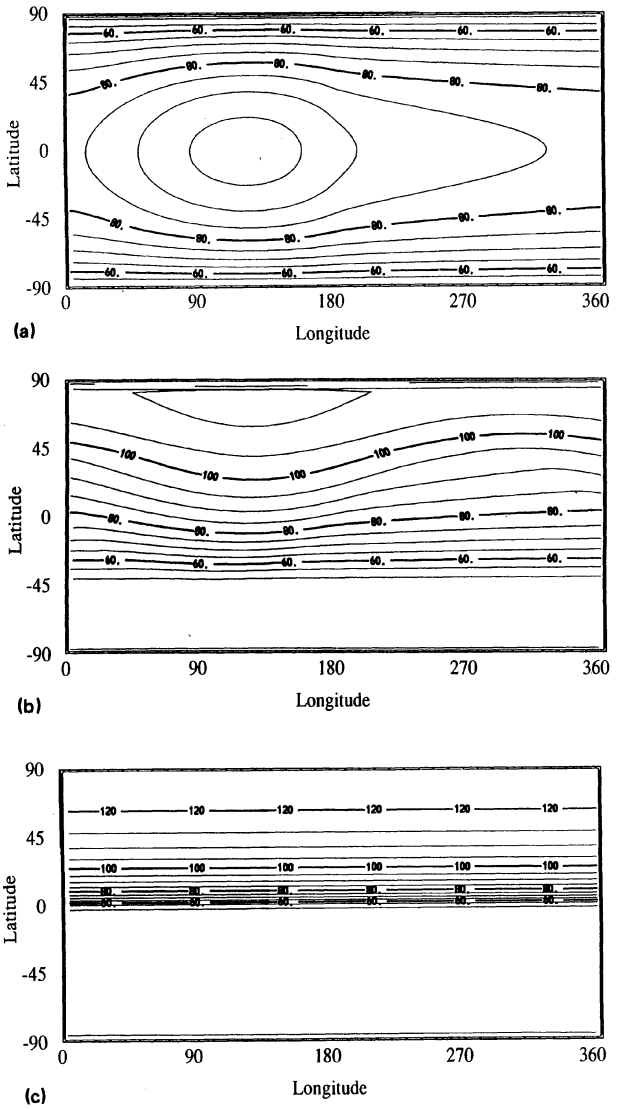

FIG. 2. Representative isotherms computed from the conduction model described in Sec. *3.2*. Isotherm maps are shown for (a) subsolar latitude 0° (Sun in the equatorial plane), (b) subsolar latitude 45°, and (c) subsolar latitude 90° (Sun on the rotation axis). The thermal inertia was taken to be $I=50\ \mathrm{J\,K^{-1}\,m^{-2}\,s^{-1/2}}$, and the model shown has $A=0.05$, $\epsilon_R=0.9$. The morning terminator is at longitude 0°, local noon at longitude 90°. The contour interval is $\Delta T=5$ K; sample contours are labeled.

was then scaled to the observational 3σ flux upper limit (Table 1) to place a limit on the diameter of 2060 Chiron. The results are summarized in Table 4. Two conclusions may be drawn from Table 4. First, the results of the conduction model are consistent with those obtained from simple considerations in Sec. *3.1*. Second, even quite extreme combinations of the unknown subsolar latitude and thermal inertia lead to modest changes in the predicted flux for a given size, and in the limiting nucleus diameter. This is because the Rayleigh–Jeans portion of the spectrum is a weak function of temperature, so that temperature differences resulting from different thermal properties and spins produce small flux differences. Thus, we conclude from Secs. *3.1* and *3.2* combined, that the 300 km limit on the

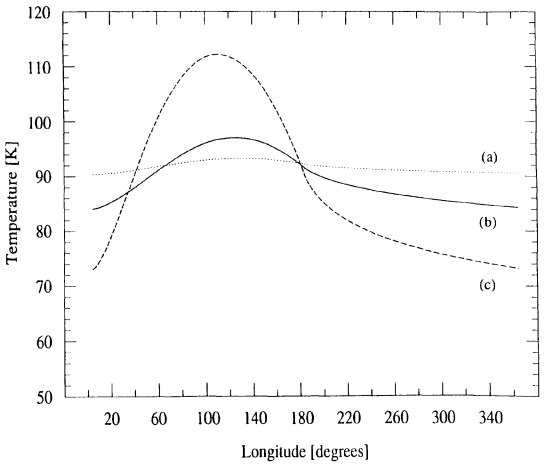

FIG. 4. Effect of thermal inertia on the equatorial diurnal surface temperature variation. Curve (a) $I=250$ J K^{-1} m^{-2} s$^{-1/2}$, (b) $I=50$ J K^{-1} m^{-2}s$^{-1/2}$, and (c) $I=10$ J K^{-1} m^{-2}s$^{-1/2}$. The models assume a Chiron subsolar latitude equal to zero. The equatorial day–night temperature contrasts for curves (a), (b), and (c) are $\Delta T\sim 2$, 12, and 40 K, respectively. Temperature contrasts at other latitudes are smaller than at the equator. Local noon occurs at longitude 90°.

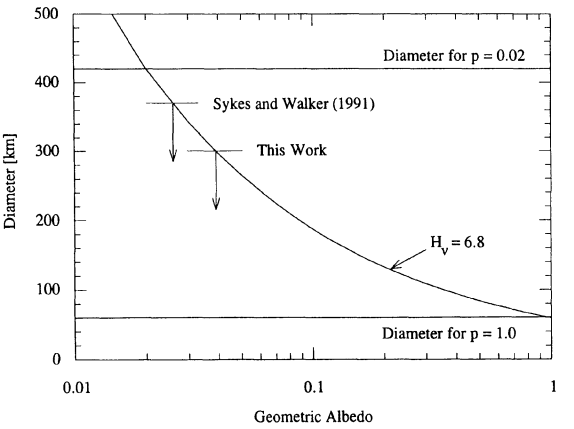

FIG. 5. Diameter-albedo constraints on 2060 Chiron. The curved line is computed from Eq. (1) with $H_v=6.8$. Horizontal lines mark diameters corresponding to $p=0.02$ and $p=1.0$, while limits from Sykes & Walker (1991) and the present 800 μm photometry are shown.

size of 2060 Chiron obtained from the 800 μm photometry is relatively robust and model independent.

4. DISCUSSION

Naturally, even the numerical conduction model of Sec. *3.2* gives only an approximate description of the temperature distribution on 2060 Chiron. The assumption that the nucleus is spheroidal may be questioned, for instance. We also neglect the possible effects of surface roughness. However, it should be noted that these effects will be less significant than in infrared data, owing to the weak temperature dependence of the Planck function in the Rayleigh–Jeans limit [Eq. (4)].

At the time of the 800 μm photometry, 2060 Chiron possessed a coma with an *optical* scattering cross section comparable to that of the nucleus (Luu & Jewitt 1990; Meech & Belton 1990). It is extremely unlikely that the coma particles contribute significantly to the 800 μm cross section, since the particles are small compared to 800 μm (Luu & Jewitt 1990), and thus fall in the Rayleigh regime for submillimeter emission. For instance, West (1991) reported an optically blue coma, which would suggest Rayleigh scattering from submicron dust. Indeed, the particles are inefficient scatterers even in the 2 μm observations of Luu & Annis (1991). Observations of other comets have shown that it is exceedingly difficult to detect submillimeter continuum from even large masses of coma particles in near-Earth comets (e.g., Altenhoff *et al.* 1988; Jewitt & Luu 1990). In any event, the presence of coma would merely strengthen the present interpretation in terms of providing a strict *upper limit* to the signal from the bare nucleus.

TABLE 4. Diameter constraints from the conduction model.

θ_{ss} (1)	I (2)	F_{800} (3)	d(km) (4)
0	10	5.4	$\leqslant$287
0	50	5.0	$\leqslant$298
0	250	4.8	$\leqslant$305
90	10	6.0	$\leqslant$272
90	50	6.0	$\leqslant$272
90	250	6.0	$\leqslant$272

Notes to TABLE 4

(1) Latitude of the subsolar point on the Chiron nucleus.
(2) Thermal inertia in MKS units (J K^{-1} m^{-2} s$^{-1/2}$).
(3) Flux density produced by the model if diameter $d=200$ km.
(4) Derived 3σ upper limit to the nucleus diameter (km).

Available constraints on the diameter of 2060 Chiron are summarized graphically in Fig. 5. The curved line in Fig. 5 shows Eq. (1), with $H_v=6.8$. Horizontal lines mark the nucleus diameters corresponding to the extreme geometric albedos $p=0.02$ and $p=1.0$. The 3σ limiting diameter from the present work is marked, as is the limiting diameter obtained by Sykes & Walker (1991). The figure shows that, in order to satisfy both the optical and the new 800 μm data, the geometric albedo must be $p\geqslant 0.04$. This limiting value would allow Chiron to be as dark as the nuclei of several short-period comets, including that of P/Halley (Keller *et al.* 1987).

Still more stringent constraints on the nature of 2060 Chiron can be expected from future submillimeter photometry. For example, in early 1993, the present single-channel bolometer, UKT14, will be supplanted by a bolometer array ("SCUBA"), in which each array element is 10 times more sensitive than UKT14 (Gear & Cunningham 1990). Coupled with the (slightly) decreasing heliocentric and geocentric distances of 2060 Chiron, it is possible that a nucleus detection will be achieved using SCUBA. For instance, a 200 km diameter nucleus would give $F_{800}\sim 5$ mJy (Table 4). Such an object could be detected in a few hours

of integration with SCUBA. Failing a diameter determination by stellar occultation, this is likely to be the most direct route to the size of the nucleus of 2060 Chiron.

5. CONCLUSIONS

(1) We have measured a 3σ upper limit to the 800 μm flux density of 2060 Chiron at $R \sim 10.5$ AU, equal to $F_{800} \leqslant 11$ mJy.

(2) This flux density limit implies a 3σ upper limit on the diameter of the nucleus of 2060 Chiron equal to $d \leqslant 300$ km. This is consistent with, but is more stringent than the 370 km upper limit to the diameter estimated by Sykes & Walker (1991) from *IRAS* photometry at 60 μm. Both limits assume emissivities $\epsilon = 0.9$. The geometric albedo needed to simultaneously match the absolute optical magnitude and the submillimeter flux limit is $p \geqslant 0.04$.

(3) The submillimeter flux imposes a strong and relatively model-independent constraint on the diameter of 2060 Chiron. Previous constraints based on shorter wavelength (infrared) photometry are subject to larger uncertainties due to the imperfectly known surface temperature distribution on Chiron.

We are grateful to JCMT telescope operators Alan Hatakeyama and Kimberly Pisciotta. We also thank our support scientist, Henry Matthews, for invariably helpful and wise utterances and for other help in the taking of the present observations. Matt Senay kindly read the manuscript; Mark Sykes provided a helpful review. This work was supported by a grant for submillimeter astronomy of comets to D. J. from the National Science Foundation, and by a Smithsonian Institution Post-Doctoral Fellowship to J. L.

REFERENCES

Altenhoff, W. J., Chini, R., Hein, H., Kreysa, E., Mezger, P. G., Salter, C., & Schraml, J. B. 1988, A&A, 190, L15
Banaszkiewicz, M., Marconi, M. L., Kömle, N. I., & Ip, W.-H. 1990, in Asteroids, Comets, Meteors III, edited by C. I. Lagerkvist, H. Rickman, B. A. Lindblad, and M. Lindgren (Uppsala University Press, Sweden), pp. 235–238
Bowell, E., Hapke, B., Domingue, D., Lumme, K., Peltoniemi, J., & Harris, A. 1989, in Asteroids II, edited by R. Binzel, T. Gehrels, and M. Matthews (University of Arizona Press, Tucson), pp. 524–556
Bus, S. J., Bowell, E., Stern, A. S. & A'Hearn, M. F. 1991 Asteroids, Comets, Meteors 1991 (submitted).
Cruikshank, D. P., & Brown, R. H. 1983, Icarus, 56, 377
Duncan, M., Quinn, T., & Tremaine, S. 1988, ApJ, 328, L69
Duncan, W. D., Robson, E. I., Ade, P. A. R., Griffin, M. J., & Sandell, G. 1990, MNRAS, 243, 126
Gear, W. K., & Cunningham, C. R. 1990, SCUBA: A Submillimetre Camera, in Proc. 29th Liége International Astrophysical Colloquium, from Ground Based to Space-Borne Sub-mm Astronomy, Liége, Belgium, 3-5 July 1990, ESA SP-314, pp. 353-358.
Hahn, G., & Bailey, M. E. 1990, Nature, 348, 132
Hartmann, W. K., Tholen, D. J., Meech, K., & Cruikshank, D. P. 1990, Icarus, 83, 1
Jewitt, D. C. 1990, ApJ, 351, 277
Jewitt, D. C., & Luu, J. X. 1990, ApJ, 365, 738
Keller, H. U., *et al.* 1987, A&A, 187, 807
Kieffer, H., Martin, T., Peterfreund, A., Jakosky, B., Miner, E., & Palluconi, F. 1977, J. Geophys. Res., 82, 4249
Lebofsky, L. A., *et al.* 1986, Icarus, 68, 239
Lebofsky, L. A., Tholen, D. J., Rieke, G. H., & Lebofsky, M. J. 1984, Icarus, 60, 532
Lunine, J., Neugebauer, G., & Jakosky, B. 1982, J. Geophys. Res., 87, 10297
Luu, J. X., & Annis, J. 1991, IAU Circ., No. 5211
Luu, J. X., & Jewitt, D. C. 1990, AJ, 100, 913
Meech, K. J., & Belton, M. J. 1990, AJ, 100, 1323
Press, W. H., Flannery, B. P., Teukolsky, S. A., & Vetterling, W. T. 1986, Numerical Recipes (Cambridge University Press, Cambridge), p. 635
Sandell, G. 1992, in preparation
Spencer, J. R., Lebofsky, L. A., & Sykes, M. V. 1989, Icarus, 78, 337
Sykes, M. V., & Walker, R. G. 1991, Science, 251, 777
Ulich, B. L., Dickel, J. R., & de Pater, I. 1984, Icarus, 60, 590
West, R. 1991, A&A, 241, 635
Winter, D., & Saari, J. 1969, ApJ, 156, 1135

PLATE 77

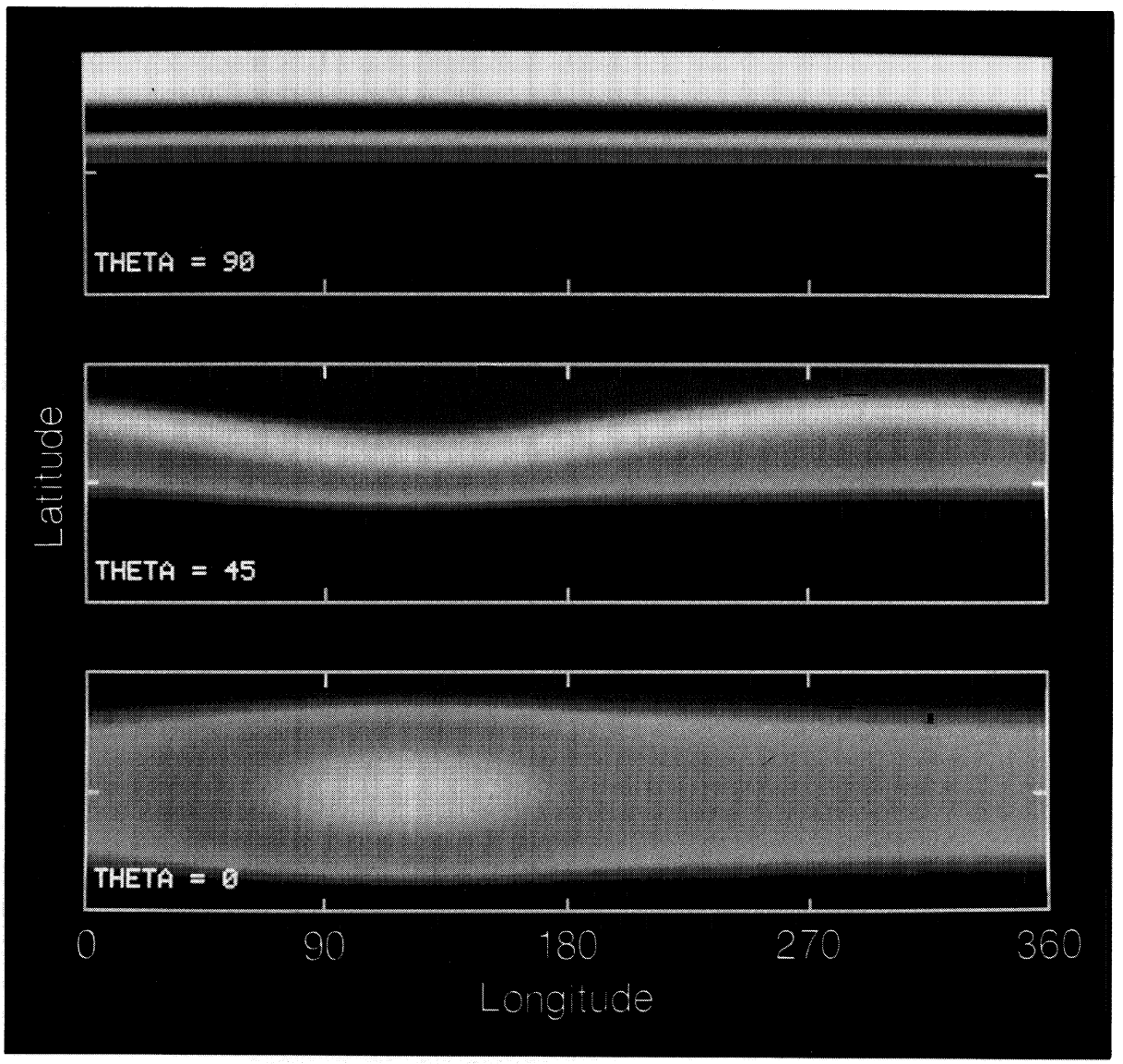

FIG. 3. The models of Fig. 2 are represented pictorially with color coding from white ($T \sim 120$ K) to blue ($T \sim 80$ K).

D. Jewitt and J. Luu (see page 402)